

Complex network model for COVID-19: human behavior, pseudo-periodic solutions and multiple epidemic waves

Cristiana J. Silva^{a,*}, Guillaume Cantin^b, Carla Cruz^a, Rui Fonseca-Pinto^c, Rui Passadouro da Fonseca^{c,d}, Estevão Soares dos Santos^d, Delfim F. M. Torres^a

^a*Center for Research and Development in Mathematics and Applications (CIDMA), Department of Mathematics, University of Aveiro, 3810-193 Aveiro, Portugal*

^b*Laboratoire de Mathématiques Appliquées, FR-CNRS-3335, 25, Rue Philippe Lebon, Le Havre Normandie 76063, France*

^c*Center for Innovative Care and Health Technology (ciTechCare), Polytechnic of Leiria, Portugal*

^d*ACES Pinhal Litoral – Central Regional Health Administration (ARS Centro), Portugal*

Abstract

We propose a mathematical model for the transmission dynamics of SARS-CoV-2 in a homogeneously mixing non constant population, and generalize it to a model where the parameters are given by piecewise constant functions. This allows us to model the human behavior and the impact of public health policies on the dynamics of the curve of active infected individuals during a COVID-19 epidemic outbreak. After proving the existence and global asymptotic stability of the disease-free and endemic equilibrium points of the model with constant parameters, we consider a family of Cauchy problems, with piecewise constant parameters, and prove the existence of pseudo-oscillations between a neighborhood of the disease-free equilibrium and a neighborhood of the endemic equilibrium, in a biologically feasible region. In the context of the COVID-19 pandemic, this pseudo-periodic solutions are related to the emergence of epidemic waves. Then, to capture the impact of mobility in the dynamics of COVID-19 epidemics, we propose a complex network with six distinct regions based on COVID-19 real data from Portugal. We perform numerical simulations for the complex network model, where the objective is to determine a topology that minimizes the level of active infected individuals and the existence of topologies that are likely to worsen the level of infection. We claim that this methodology is a tool with enormous potential in the current pandemic context, and can be applied in the management of outbreaks (in regional terms) but also to manage the opening/closing of borders.

Keywords: COVID-19 epidemic waves, piecewise constant parameters, pseudo-periodic solutions, complex network, Portugal case study

2020 MSC: 92D30 (Primary), 05C82, 34C60, 34D20 (Secondary)

1. Introduction

The history of the pandemics that have already plagued mankind has revealed that there are consistently periods of marked increase in infected individuals, followed by phases in which the

*Corresponding author

Email addresses: cjoaosilva@ua.pt (Cristiana J. Silva), guillaumecantin@mail.com (Guillaume Cantin), carla.cruz@ua.pt (Carla Cruz), rui.pinto@ipleiria.pt (Rui Fonseca-Pinto), rmfonseca@arscentro.min-saude.pt (Rui Passadouro da Fonseca), essantos3@arscentro.min-saude.pt (Estevão Soares dos Santos), delfim@ua.pt (Delfim F. M. Torres)

URL: <https://orcid.org/0000-0002-7238-546X> (Cristiana J. Silva), <https://orcid.org/0000-0001-5122-1194> (Guillaume Cantin), <https://orcid.org/0000-0003-4082-7523> (Carla Cruz), <https://orcid.org/0000-0001-6774-5363> (Rui Fonseca-Pinto), <https://orcid.org/0000-0002-7766-576X> (Rui Passadouro da Fonseca), <https://orcid.org/0000-0001-6567-1487> (Estevão Soares dos Santos), <https://orcid.org/0000-0001-8641-2505> (Delfim F. M. Torres)

numbers are relatively lower. In these cases, there is also a repetition of these oscillations that are called pandemic waves. A second wave of the pandemic poses an imminent threat to society, with an immense cost in terms of human lives and a devastating economic impact, it is therefore, crucial to try to avoid the emergence of pandemic waves.

The coronavirus disease 2019 (COVID-19) is an infectious disease caused by the severe acute respiratory syndrome coronavirus-2 (SARS-CoV-2). The World Health Organization announced the COVID-19 outbreak as a pandemic on 11 March 2020 [19]. At the time of writing, several countries across Europe are seeing a resurgence in COVID-19 cases after successfully controlling the first outbreak and started to take action to face the so-called second wave [10]. Mathematical tools have been important in the analysis and control of COVID-19 pandemic, see e.g. [15, 22, 18, 17] and references cited therein.

In this paper, we propose a mathematical model given by a system of ordinary equations based on the model from [23], for the transmission dynamics of SARS-CoV-2 in a homogeneously mixing population, and we generalize it to a non constant population model with piecewise constant parameters. Considering parameters determined by piecewise constant functions allows to model the governmental and public health decisions of political actors, which have a large influence on the behaviors of individuals, which in turn can change the dynamics of the epidemic, see e.g. [1, 4, 9]. Moreover, the piecewise constant parameters also allows to mathematical model the human behavior in the application of non-pharmaceutical interventions (NPI), such as, physical distancing, limited size of indoor and outdoor gatherings, teleworking, regular cleaning of frequently-touched surfaces and appropriate ventilation of indoor spaces, mask use, avoiding close contact and hand washing, see e.g. [11, 12].

Viruses need cells to replicate themselves, as they are not able to do so on their own. Depending on the type of virus, contagion is more or less facilitated depending on the means of transmission. In the case of SARS-COV-2, the transmission is carried out through droplets containing viruses that are sent from the respiratory tract. Accordingly, as the airways are the gateway to the virus, the proximity of people and the dynamics imposed by the movement are a determining factor in the spread of the COVID-19 disease. The proof that the movement of people is a determining factor for contagion is that during the recent periods of confinement the number of infections has decreased very markedly [26].

In this paper, the COVID-19 mathematical model is improved by constructing a complex network of dynamical systems, following the framework presented in [6, 7], in order to take into account the mobilities of individuals, which are also known to play a decisive role in the dynamics of the epidemic. We investigate in which cases such a COVID-19 second wave can occur, by establishing sufficient conditions for pseudo-periodic solutions: see, e.g., [8, 27, 14] for traveling waves results in epidemiological models and [3, 5, 13] for complex network models.

Our model is calibrated in order to fit with the real data of the COVID-19 dynamics in six regions of Portugal mainland, namely *Norte*, *Centro*, *Lisboa e Vale do Tejo*, *Alentejo*, *Algarve* and *Pinhal Litoral*.

Numerical simulations are provided where we explore the effect of the topology of the network on the dynamics of the epidemics (disposal of connections and coupling strength). We identify which type of topology minimizes the level of infection of the epidemic, and which type of topology worsens the number of infected individuals.

This paper is organized as follows. In Section 2, we propose a mathematical model for the transmission dynamics of SARS-COV-2, with constant parameters and variable population size. We show that the model admits two equilibrium points and analyze their local and global stability. In Section 3, we consider piecewise constant parameters, which allows to model the impact of public health policies and the human behavior in the dynamics of the COVID-19 epidemic. The existence and uniqueness of global solutions of the model with piecewise constant parameters is proved. An important result in the context of the COVID-19 pandemic and the resurgence of epidemic waves, is proved in Section 4, where a sufficient condition is proved to the existence of pseudo-periodic solutions. In Section 5, we construct a complex network of *SAIRP* models with piecewise constant parameters, where each node represent one of six regions in Portugal, and where the values of the parametes differ from one region to another. The case study, with COVID-19 real data from

Portugal, is analyzed in Section 6, where we calibrate the model to each of the six regions and after, numerical simulations are performed in order to determine the topologies that minimizes the average number of active infected individuals in Portugal. The results obtained in this paper are discussed, in Section 7, from a practical point of view and its implications in the management of the COVID-19 pandemic waves. We end the paper in Section 8, with some conclusions and future work.

2. Model with constant parameters

We propose a compartmental *SAIRP* mathematical model, based on [23], where the population is subdivided into five classes: susceptible individuals (S); asymptomatic infected individuals (A); active infected individuals (I); removed (including recovered and COVID-19 induced deaths) (R); protected individuals (P). The total population, $N(t) = S(t) + A(t) + I(t) + R(t) + P(t)$, with $t \in [0, T]$ representing the time (in days) and $T > 0$, has a variable size where the recruitment rate, Λ , and the natural death rate, $\mu > 0$, are assumed to be constant. The susceptible individuals S become infected by contact with active infected I and asymptomatic infected A individuals, at a rate of infection $\beta \frac{(\theta A + I)}{N}$, where θ represents a modification parameter for the infectiousness of the asymptomatic infected individuals A . The remaining assumptions follows the one from [23]: only a fraction q of asymptomatic infected individuals A develop symptoms and are detected, at a rate ν . Active infected individuals I are transferred to the recovered/removed individuals R , at a rate δ , by recovery from the disease or by COVID-19 induced death. A fraction p , with $0 < p < 1$, is protected (not immune) from infection, by the application of non-pharmaceutical interventions (NPI), such as, physical distancing, limited size of indoor and outdoor gatherings, teleworking, regular cleaning of frequently-touched surfaces and appropriate ventilation of indoor spaces, mask use and hand washing, see e.g. [11, 12], that prevent from being exposed to the infection, and is transferred to the class of protected individuals P , at a rate ϕ . A fraction m of protected individuals P returns to the susceptible class S , at a rate w . In what follows, for the sake of simplification, we use the notation $\nu = \nu q$ and $\omega = wm$. The previous assumptions are described by the following system:

$$\begin{cases} \dot{S}(t) = \Lambda - \beta(1-p) \frac{(\theta A(t) + I(t))}{N(t)} S(t) - \phi p S(t) + \omega P(t) - \mu S(t), \\ \dot{A}(t) = \beta(1-p) \frac{(\theta A(t) + I(t))}{N(t)} S(t) - \nu A(t) - \mu A(t), \\ \dot{I}(t) = \nu A(t) - \delta I(t) - \mu I(t), \\ \dot{R}(t) = \delta I(t) - \mu R(t), \\ \dot{P}(t) = \phi p S(t) - \omega P(t) - \mu P(t). \end{cases} \quad (1)$$

2.1. Existence, positivity and boundedness of solutions

The equations of the SAIRP model (1) can be rewritten as

$$\dot{x}(t) = f(x(t), \alpha), \quad t > 0, \quad (2)$$

with $x = (S, A, I, R, P)^T \in \mathbb{R}^5$ and $\alpha = (\Lambda, \mu, \beta, p, \theta, \phi, \omega, \nu, \delta)^T \in \mathbb{R}^9$, where the non-linear operator f is defined in $\mathbb{R}^5 \times \mathbb{R}^9$ by

$$f(x, \alpha) = \begin{pmatrix} \Lambda - \beta(1-p) \frac{(\theta A + I)}{N} - \phi p S + \omega P - \mu S \\ \beta(1-p) \frac{(\theta A + I)}{N} S - \nu A - \mu A \\ \nu A - \delta I - \mu I \\ \delta I - \mu R \\ \phi p S - \omega P - \mu P \end{pmatrix}. \quad (3)$$

In order to prove that the problem determined by (2) is well-posed, we introduce the compact region $\Omega \subset \mathbb{R}^5$ defined by

$$\Omega = \left\{ x = (S, A, I, R, P)^T \in (\mathbb{R}^+)^5 ; 0 < S + A + I + R + P \leq \frac{\Lambda}{\mu} \right\}. \quad (4)$$

The following theorem establishes the existence of global solutions to (2).

Theorem 1. *For any $x_0 = (S_0, A_0, I_0, R_0, P_0)^T \in \Omega$, the Cauchy problem given by (2) and $x(0) = x_0$ admits a unique solution, denoted by $x(t, x_0)$, defined on $[0, \infty)$, whose components are non-negative. Furthermore, the region Ω defined by (4) is positively invariant.*

Proof. The existence of a local in time solution $x(t, x_0)$ to problem (2) starting from $x_0 \in \Omega$ follows from the theory of ordinary equations (see, for instance, [20]). The non-negativity of the components is guaranteed by the quasi-positivity of the non-linear operator $f = (f_j)_{1 \leq j \leq 5}$, which means that it satisfies the property

$$f_i(x_1, \dots, x_{i-1}, 0, x_{i+1}, \dots, x_5, \alpha) \geq 0,$$

for all $x = (x_1, \dots, x_5) \in (\mathbb{R}^+)^5$, $i \in \{1, \dots, 5\}$ and $\alpha \in \mathbb{R}^9$. By virtue of Proposition A.17 in [24], it follows that the components of any solution $x(t, x_0)$ stemming from x_0 in Ω remain non-negative in future time. Finally, summing the five equations of system (2) leads to

$$\dot{N}(t) + \mu N(t) \leq \Lambda, \quad t > 0,$$

from which it is deduced, using Gronwall's lemma, that

$$N(t) \leq \left[N(0) - \frac{\Lambda}{\mu} \right] e^{-\mu t} + \frac{\Lambda}{\mu}, \quad t > 0.$$

The latter inequality proves that the region Ω defined by (4) is positively invariant. \square

2.2. Equilibrium points and basic reproduction number

In this section, we study the equilibrium points of system (1) and derive their expressions with respect to the parameters of the model. We compute the basic reproduction number, denoted by R_0 , following the approach in [25].

Proposition 1. *The model (1) has two equilibrium points:*

- *disease-free equilibrium, denoted by Σ_0 , given by*

$$\Sigma_0 = (S_0, A_0, I_0, R_0, P_0) = \left(\frac{\Lambda(\omega + \mu)}{\mu(p\phi + \mu + \omega)}, 0, 0, 0, \frac{\phi p \Lambda}{\mu(p\phi + \mu + \omega)} \right); \quad (5)$$

- *endemic equilibrium, Σ_+ , whenever $R_0 > 1$, given by*

$$\Sigma_+ = (S_+, A_+, I_+, R_+, P_+) \quad (6)$$

with

$$\begin{aligned} S_+ &= \frac{\Lambda(\omega + \mu)}{(p\phi + \mu + \omega)\mu} R_0^{-1}, \\ A_+ &= \frac{\Lambda}{\nu + \mu} R_0^{-1} (R_0 - 1), \\ I_+ &= \frac{\Lambda\nu}{(\nu + \mu)(\delta + \mu)} R_0^{-1} (R_0 - 1), \\ R_+ &= \frac{\delta\Lambda\nu}{(\nu + \mu)(\delta + \mu)\mu} R_0^{-1} (R_0 - 1), \\ P_+ &= \frac{\Lambda\phi p}{(p\phi + \mu + \omega)\mu} R_0^{-1}, \end{aligned} \quad (7)$$

where the basic reproduction number, R_0 , is given by

$$R_0 = \frac{\beta (1-p) (\delta \theta + \mu \theta + \nu) (\omega + \mu)}{(\delta + \mu) (\nu + \mu) (p\phi + \mu + \omega)} = \frac{\mathcal{N}}{\mathcal{D}}. \quad (8)$$

Proof. The computation of the equilibrium points and the basic reproduction number follows standard arguments, see [25]. \square

2.3. Local and global stability analysis

In what follows we prove the local and global asymptotic stability of the disease-free equilibrium (DFE), when the basic reproduction number satisfies the inequality $R_0 < 1$. For $R_0 > 1$, we prove that the endemic equilibrium is globally asymptotically stable in a biologically meaningful compact positive invariant region.

Theorem 2 (local stability of the DFE). *The disease-free equilibrium, Σ_0 , is locally asymptotically stable whenever $R_0 < 1$.*

Proof. The Jacobian matrix of system (1), evaluated at the disease-free equilibrium (5), is given by

$$M(\Sigma_0) = \begin{bmatrix} -(\phi p + \mu) & -\frac{\theta \beta (\mu + \omega)(1-p)}{\phi p + \mu + \omega} & -\frac{\beta (\mu + \omega)(1-p)}{\phi p + \mu + \omega} & 0 & \omega \\ 0 & -\frac{\beta \theta (1-p)(\mu + \omega) + (\mu + \nu)(p\phi + \mu + \omega)}{\phi p + \mu + \omega} & \frac{\beta (\mu + \omega)(1-p)}{\phi p + \mu + \omega} & 0 & 0 \\ 0 & \nu & -\delta - \mu & 0 & 0 \\ 0 & 0 & \delta & -\mu & 0 \\ \phi p & 0 & 0 & 0 & -(\mu + \omega) \end{bmatrix}.$$

The eigenvalues of the matrix $M(\Sigma_0)$ are given by $\lambda_1 = \lambda_2 = -\mu$, $\lambda_3 = -(\phi p + \mu + \omega)$ and the remaining two, λ_4 and λ_5 , are the roots of the polynomial $p(\lambda)$ given by

$$p(\lambda) = \lambda^2 + B\lambda + C,$$

where $B = \frac{-\beta \theta (1-p)(\omega + \mu)}{p\phi + \mu + \omega} + \delta + 2\mu + \nu$ and $C = \frac{\mathcal{D} - \mathcal{N}}{p\phi + \mu + \omega}$. Applying the Routh–Hurwitz criterion, we conclude that model (1) is locally stable if, and only if, $A > 0$ and $B > 0$. It is easy to show that $C > 0$ whenever $R_0 < 1$. The coefficient B is positive when

$$\beta \theta (1-p)(\omega + \mu) < (\delta + 2\mu + \nu)(p\phi + \mu + \omega).$$

Since all parameters take positive values, we have

$$\beta \theta (1-p)(\omega + \mu) < \underbrace{\beta (1-p) (\delta \theta + \mu \theta + \nu) (\omega + \mu)}_{\mathcal{N}}.$$

From $R_0 < 1$, we have $\mathcal{N} < \mathcal{D}$ and, therefore,

$$\underbrace{\beta (1-p) (\delta \theta + \mu \theta + \nu) (\omega + \mu)}_{\mathcal{N}} < \underbrace{(\delta + \mu) (\nu + \mu) (p\phi + \mu + \omega)}_{\mathcal{D}}.$$

From the biological meaning of δ , μ and ν , we have that $0 < \delta, \mu, \nu < 1$ (observe that their unit is day^{-1}). Therefore,

$$0 < \delta + \mu < 2 \quad \text{and} \quad 0 < \mu + \nu < 2$$

and

$$\frac{1}{\delta + \mu} > \frac{1}{2} \quad \text{and} \quad \frac{1}{\mu + \nu} > \frac{1}{2},$$

that is,

$$\frac{1}{\delta + \mu} + \frac{1}{\mu + \nu} > 1.$$

Multiplying the previous inequality by $(\delta + \mu)(\mu + \nu)$ we have

$$\left(\frac{1}{\delta + \mu} + \frac{1}{\mu + \nu} \right) (\delta + \mu)(\mu + \nu) > (\delta + \mu)(\mu + \nu).$$

In other words,

$$(\delta + \mu)(\mu + \nu) < \delta + 2\mu + \nu.$$

Therefore,

$$(\delta + \mu)(\nu + \mu)(p\phi + \mu + \omega) < (\delta + 2\mu + \nu)(p\phi + \mu + \omega),$$

which ensures that $B > 0$. It follows the local asymptotic stability of the disease-free equilibrium Σ_0 . \square

Theorem 3 (global stability of the DFE). *If $R_0 < 1$, then the disease-free equilibrium, Σ_0 , is globally asymptotically stable in Ω .*

Proof. Since $R_0 < 1$, we can write $R_0 = 1 - \eta$ with $0 < \eta < 1$. We obtain that

$$\frac{\beta(1-p)(\delta\theta + \mu\theta + \nu)(\omega + \mu)}{(\delta + \mu)(\nu + \mu)(p\phi + \mu + \omega)} = 1 - \eta,$$

which leads to

$$\frac{\beta(1-p)(\delta\theta + \mu\theta + \nu)}{(\delta + \mu)(\nu + \mu)} = k(1 - \eta), \quad (9)$$

where k is defined by

$$k = \frac{p\phi + \mu + \omega}{\mu + \omega}.$$

A fortiori, we have:

$$\frac{\beta(1-p)\theta}{\nu + \mu} < k(1 - \eta). \quad (10)$$

Now we consider the following functional given by

$$L = S - S_0 - S_0 \ln \frac{S}{S_0} + A + \zeta I + \xi \left(P - P_0 - P_0 \ln \frac{P}{P_0} \right) + \chi \left(N - N_0 - N_0 \ln \frac{N}{N_0} \right),$$

where ζ and ξ are defined by

$$\zeta = \frac{k(1-\eta)(\nu + \mu) - \beta(1-p)\theta}{k\nu(1-\eta)}, \quad \xi = \frac{\omega P_0}{\phi p S_0}, \quad (11)$$

and χ is a positive constant which will be determined below. Recall that $N_0 = \frac{\Lambda}{\mu}$, and note that $\zeta > 0$ by virtue of (10). As constructed, L is a non-negative functional and we have

$$L = 0 \iff (S, A, I, R, P) = \Sigma_0.$$

Now we compute the derivative of L along the solutions of the SAIRP model (1) starting in Ω . We have

$$\begin{aligned} \dot{L} &= \left(1 - \frac{S_0}{S} \right) \dot{S} + \dot{A} + \zeta \dot{I} + \xi \left(1 - \frac{P_0}{P} \right) \dot{P} + \chi \left(1 - \frac{N_0}{N} \right) \dot{N} \\ &= \left(1 - \frac{S_0}{S} \right) \left[\Lambda - \beta(1-p) \frac{\theta A + I}{N} S - (p\phi + \mu) S + \omega P \right] \\ &\quad + \left[\beta(1-p) \frac{\theta A + I}{N} S - (\nu + \mu) A \right] + \zeta [\nu A - (\delta + \mu) I] \\ &\quad + \xi \left(1 - \frac{P_0}{P} \right) [\phi p S - (\omega + \mu) P] + \chi \left(1 - \frac{N_0}{N} \right) (\Lambda - \mu N). \end{aligned}$$

Now we use the relations

$$\Lambda = (p\phi + \mu)S_0 - \omega P_0, \quad p\phi S_0 = (\omega + \mu)P_0$$

to obtain

$$\begin{aligned} \dot{L} &= \left(1 - \frac{S_0}{S}\right) \left[-\beta(1-p) \frac{\theta A + I}{N} S - (p\phi + \mu)(S - S_0) + \omega(P - P_0) \right] \\ &\quad + \left[\beta(1-p) \frac{\theta A + I}{N} S - (\nu + \mu)A \right] + \zeta [\nu A - (\delta + \mu)I] \\ &\quad + \xi \left(1 - \frac{P_0}{P}\right) [\phi p(S - S_0) - (\omega + \mu)(P - P_0)] + \chi \left(1 - \frac{N_0}{N}\right) (\Lambda - \mu N). \end{aligned}$$

First step. Let us examine the terms involving $(S - S_0)$ and $(P - P_0)$. We have

$$\begin{aligned} \Theta_1 &= - (p\phi + \mu) \left(1 - \frac{S_0}{S}\right) (S - S_0) + \omega \left(1 - \frac{S_0}{S}\right) (P - P_0) \\ &\quad + \xi p\phi \left(1 - \frac{P_0}{P}\right) (S - S_0) - \xi(\omega + \mu) \left(1 - \frac{P_0}{P}\right) (P - P_0) \\ &= - (p\phi + \mu)S_0 \left(1 - \frac{S_0}{S}\right) \left(\frac{S}{S_0} - 1\right) + \omega P_0 \left(1 - \frac{S_0}{S}\right) \left(\frac{P}{P_0} - 1\right) \\ &\quad + \xi p\phi S_0 \left(1 - \frac{P_0}{P}\right) \left(\frac{S}{S_0} - 1\right) - \xi(\omega + \mu)P_0 \left(1 - \frac{P_0}{P}\right) \left(\frac{P}{P_0} - 1\right) \\ &= - (p\phi + \mu)S_0 \left(\frac{S_0}{S} + \frac{S}{S_0} - 2\right) + \omega P_0 \left[\left(\frac{P}{P_0} + \frac{S_0}{S} - 2\right) + \left(1 - \frac{P}{P_0} \times \frac{S_0}{S}\right)\right] \\ &\quad + \xi p\phi S_0 \left[\left(\frac{S}{S_0} + \frac{P_0}{P} - 2\right) + \left(1 - \frac{S}{S_0} \times \frac{P_0}{P}\right)\right] - \xi(\omega + \mu)P_0 \left(\frac{P_0}{P} + \frac{P}{P_0} - 2\right). \end{aligned}$$

Now we have chosen ξ such that $\omega P_0 = \xi p\phi S_0$. The latter equality becomes

$$\begin{aligned} \Theta_1 &= - (p\phi + \mu)S_0 \left(\frac{S_0}{S} + \frac{S}{S_0} - 2\right) + \omega P_0 \left(\frac{P}{P_0} + \frac{S_0}{S} - 2\right) + \omega P_0 \left(1 - \frac{P}{P_0} \times \frac{S_0}{S}\right) \\ &\quad + \omega P_0 \left(1 - \frac{S}{S_0} \times \frac{P_0}{P}\right) + \omega P_0 \left(\frac{S}{S_0} + \frac{P_0}{P} - 2\right) - \xi(\omega + \mu)P_0 \left(\frac{P_0}{P} + \frac{P}{P_0} - 2\right) \\ &= [-(p\phi + \mu)S_0 + \omega P_0] \left(\frac{S_0}{S} + \frac{S}{S_0} - 2\right) + [\omega P_0 - \xi(\omega + \mu)P_0] \left(\frac{P_0}{P} + \frac{P}{P_0} - 2\right) \\ &\quad + \omega P_0 \left(2 - \frac{S_0 S^{-1}}{P_0 P^{-1}} - \frac{P_0 P^{-1}}{S_0 S^{-1}}\right). \end{aligned}$$

Elementary computations show that

$$-(p\phi + \mu)S_0 + \omega P_0 < 0, \quad \omega P_0 - \xi(\omega + \mu)P_0 = 0.$$

Now we use the standard inequality

$$2 - x - \frac{1}{x} \leq 0, \quad \forall x > 0,$$

to conclude that $\Theta_1 \leq 0$. Thus, we obtain

$$\begin{aligned} \dot{L} &\leq \left(1 - \frac{S_0}{S}\right) \left[-\beta(1-p) \frac{\theta A + I}{N} S \right] + \left[\beta(1-p) \frac{\theta A + I}{N} S - (\nu + \mu)A \right] \\ &\quad + \zeta [\nu A - (\delta + \mu)I] + \chi \left(1 - \frac{N_0}{N}\right) (\Lambda - \mu N). \end{aligned}$$

Second step. We examine the terms involving A and I . After simplifications, we have

$$\begin{aligned}
\dot{L} &\leq \beta(1-p)\theta A \left[\frac{S_0}{N} - \frac{(\nu + \mu) - \zeta\nu}{\beta(1-p)\theta} \right] + \beta(1-p)I \left[\frac{S_0}{N} - \frac{\zeta(\delta + \mu)}{\beta(1-p)} \right] - \chi\mu \frac{(N - N_0)^2}{N} \\
&\leq \beta(1-p)\theta A \left[\frac{S_0}{N_0} - \frac{(\nu + \mu) - \zeta\nu}{\beta(1-p)\theta} \right] + \beta(1-p)I \left[\frac{S_0}{N_0} - \frac{\zeta(\delta + \mu)}{\beta(1-p)} \right] \\
&\quad + \beta(1-p)\theta A \left(\frac{S_0}{N} - \frac{S_0}{N_0} \right) - \frac{\chi}{2}\mu \frac{(N - N_0)^2}{N} \\
&\quad + \beta(1-p)I \left(\frac{S_0}{N} - \frac{S_0}{N_0} \right) - \frac{\chi}{2}\mu \frac{(N - N_0)^2}{N}.
\end{aligned}$$

Next, we write

$$\Theta_2 = \beta(1-p)\theta A \left(\frac{S_0}{N} - \frac{S_0}{N_0} \right) - \frac{\chi}{2}\mu \frac{(N - N_0)^2}{N} = \frac{\beta(1-p)\theta S_0}{NN_0} A(N_0 - N) - \frac{\chi}{2}\mu \frac{(N - N_0)^2}{N}.$$

By virtue of Young's inequality, we have

$$A(N_0 - N) \leq \frac{\varepsilon A^2}{2} + \frac{(N_0 - N)^2}{2\varepsilon},$$

where ε is a positive coefficient which can be chosen arbitrarily small. It follows that

$$\begin{aligned}
\Theta_2 &\leq \frac{\beta(1-p)\theta S_0}{NN_0} \left[\frac{\varepsilon A^2}{2} + \frac{(N_0 - N)^2}{2\varepsilon} \right] - \frac{\chi}{2}\mu \frac{(N - N_0)^2}{N} \\
&\leq \beta(1-p)\theta \frac{A}{N} \times A \times \frac{\varepsilon S_0}{2N_0} + \left[\frac{\beta(1-p)\theta S_0}{2N_0\varepsilon} - \frac{\chi}{2}\mu \right] \frac{(N - N_0)^2}{N}.
\end{aligned}$$

Since $A \leq N$, we obtain

$$\Theta_2 \leq \beta(1-p)\theta \times A \times \frac{\varepsilon S_0}{2N_0} + \left[\frac{\beta(1-p)\theta S_0}{2N_0\varepsilon} - \frac{\chi}{2}\mu \right] \frac{(N - N_0)^2}{N}.$$

Similar computations show that

$$\beta(1-p)I \left(\frac{S_0}{N} - \frac{S_0}{N_0} \right) - \frac{\chi}{2}\mu \frac{(N - N_0)^2}{N} \leq \beta(1-p) \times I \times \frac{\varepsilon S_0}{2N_0} + \left[\frac{\beta(1-p)S_0}{2N_0\varepsilon} - \frac{\chi}{2}\mu \right] \frac{(N - N_0)^2}{N}.$$

We obtain that

$$\begin{aligned}
\dot{L} &\leq \beta(1-p)\theta A \left[\frac{S_0}{N_0} \left(1 + \frac{\varepsilon}{2} \right) - \frac{(\nu + \mu) - \zeta\nu}{\beta(1-p)\theta} \right] + \beta(1-p)I \left[\frac{S_0}{N_0} \left(1 + \frac{\varepsilon}{2} \right) - \frac{\zeta(\delta + \mu)}{\beta(1-p)} \right] \\
&\quad + \left[\frac{\beta(1-p)\theta S_0}{2N_0\varepsilon} - \frac{\chi}{2}\mu \right] \frac{(N - N_0)^2}{N} + \left[\frac{\beta(1-p)S_0}{2N_0\varepsilon} - \frac{\chi}{2}\mu \right] \frac{(N - N_0)^2}{N}.
\end{aligned}$$

Now we choose

$$\varepsilon = \frac{2\eta}{1-\eta} = \frac{2(1-R_0)}{R_0} > 0,$$

which yields $1 + \frac{\varepsilon}{2} = \frac{1}{1-\eta}$. Since $\frac{S_0}{N_0} = \frac{1}{k}$, we obtain, by virtue of (11),

$$\frac{S_0}{N_0} \left(1 + \frac{\varepsilon}{2} \right) - \frac{(\nu + \mu) - \zeta\nu}{\beta(1-p)\theta} = \frac{1}{k(1-\eta)} - \frac{(\nu + \mu) - \zeta\nu}{\beta(1-p)\theta} = 0.$$

Analogously, it is seen that

$$\begin{aligned}
\frac{S_0}{N_0} \left(1 + \frac{\varepsilon}{2} \right) - \frac{\zeta(\delta + \mu)}{\beta(1-p)} &= \frac{1}{k(1-\eta)} - \frac{\zeta(\delta + \mu)}{\beta(1-p)} \\
&= \frac{\beta(1-p)(\theta\delta + \theta\mu + \nu) - k(1-\eta)(\nu + \mu)(\delta + \mu)}{\beta(1-p)\nu k(1-\eta)} = 0,
\end{aligned}$$

by virtue of (9). After those simplifications, we obtain

$$\begin{aligned}\dot{L} &\leq \left[\frac{\beta(1-p)\theta S_0}{2N_0\varepsilon} - \frac{\chi}{2}\mu \right] \frac{(N-N_0)^2}{N} + \left[\frac{\beta(1-p)S_0}{2N_0\varepsilon} - \frac{\chi}{2}\mu \right] \frac{(N-N_0)^2}{N} \\ &\leq \left[\frac{\beta(1-p)S_0}{N_0\varepsilon} - \chi\mu \right] \frac{(N-N_0)^2}{N},\end{aligned}$$

since $\theta \leq 1$. Finally, we choose $\chi > 0$ sufficiently large so that

$$\frac{\beta(1-p)S_0}{N_0\varepsilon} - \chi\mu < 0,$$

which guarantees that $\dot{L} \leq 0$. In other words, the functional L is a Lyapunov function for the flow induced by the SAIRP model (1). The conclusion follows from LaSalle's invariance principle [16]. \square

The next theorem establishes the global stability of the endemic equilibrium (EE) Σ_+ defined by (7), in an invariant region $\Gamma \subset \Omega$. It remains an open question to determine if the endemic equilibrium is globally asymptotically stable in the whole region Ω .

Theorem 4 (global stability of the EE). *The compact region Γ defined by*

$$\Gamma = \left\{ x = (S, A, I, R, P)^T \in (\mathbb{R}^+)^5 ; S + A + I + R + P = \frac{\Lambda}{\mu} \right\} \quad (12)$$

is positively invariant under the flow induced by system (1). It contains the disease-free equilibrium, Σ_0 , and the endemic equilibrium, Σ_+ , if $R_0 > 1$. Furthermore, if $R_0 > 1$, then the endemic equilibrium Σ_+ is globally asymptotically stable in Γ .

Proof. Let us first prove that Γ is positively invariant under the flow induced by system (1). We denote by $x(t, x_0) = (S(t), A(t), I(t), R(t), P(t))$ the solution of system (1) starting from $x_0 \in \Gamma$. Summing again the five equations of system (1) leads to

$$\dot{N}(t) + \mu N(t) = \Lambda, \quad t > 0,$$

where $N(t) = S(t) + A(t) + I(t) + R(t) + P(t)$. Consequently, we have

$$N(t) = \left[N(0) - \frac{\Lambda}{\mu} \right] e^{-\mu t} + \frac{\Lambda}{\mu}, \quad t > 0.$$

Now we have $N(0) = \frac{\Lambda}{\mu}$ since $x_0 \in \Gamma$. It follows that $N(t) = \frac{\Lambda}{\mu}$ for all $t > 0$, which proves that Γ is positively invariant. Next, we easily verify that Σ_0 and Σ_+ belong to Γ . Now we turn to prove the global stability of Σ_+ in Γ . To that aim, we introduce the functional V defined by

$$\begin{aligned}V &= c_1 \left(S - S_+ - S_+ \ln \frac{S}{S_+} \right) + c_2 \left(A - A_+ - A_+ \ln \frac{A}{A_+} \right) \\ &\quad + c_3 \left(I - I_+ - I_+ \ln \frac{I}{I_+} \right) + c_4 \left(P - P_+ - P_+ \ln \frac{P}{P_+} \right),\end{aligned} \quad (13)$$

with positive coefficients c_1, c_2, c_3 , and c_4 satisfying

$$c_1 = c_2, \quad c_1\omega P_+ = c_4 p \phi S_+, \quad c_3\nu A_+ = c_1\beta(1-p)\frac{S_+ I_+}{N_+}, \quad (14)$$

where $N_+ = \frac{\Lambda}{\mu}$. As constructed, V is a non-negative functional and we have

$$V = 0 \iff (S, A, I, R, P) = \Sigma_+.$$

We compute the time derivative of V along the solutions of system (1) starting in Γ . Using the fact that Σ_+ is an equilibrium of system (1), we obtain, after simplifications, that

$$\begin{aligned}\dot{V} = & c_1 \left(1 - \frac{S_+}{S}\right) \left[\beta(1-p) \frac{\theta A_+ + I_+}{N_+} S_+ - \beta(1-p) \frac{\theta A + I}{N_+} S + \omega(P - P_+) - (p\phi + \mu)(S - S_+) \right] \\ & + c_2 \left(1 - \frac{A_+}{A}\right) \left[\beta(1-p) \frac{\theta A + I}{N_+} S - \beta(1-p) \frac{\theta A_+ + I_+}{N_+} S_+ - (\nu + \mu)(A - A_+) \right] \\ & + c_3 \left(1 - \frac{I_+}{I}\right) [\nu(A - A_+) - (\delta + \mu)(I - I_+)] \\ & + c_4 \left(1 - \frac{P_+}{P}\right) [p\phi(S - S_+) - (\omega + \mu)(P - P_+)].\end{aligned}$$

We perform elementary computations, so as to split \dot{V} into four terms, as follows:

$$\dot{V} = \Phi_1 + \Phi_2 + \Phi_3 + \Phi_4,$$

with

$$\begin{aligned}\Phi_1 = & c_1 \left(1 - \frac{S_+}{S}\right) [\omega(P - P_+) - (p\phi + \mu)(S - S_+)] \\ & + c_4 \left(1 - \frac{P_+}{P}\right) [p\phi(S - S_+) - (\omega + \mu)(P - P_+)], \\ \Phi_2 = & -c_1 \beta(1-p) \theta \frac{S_+ A_+}{N_+} \left(\frac{S}{S_+} + \frac{S_+}{S} - 2\right), \\ \Phi_3 = & -c_3(\delta + \mu) I_+ \left(\frac{I}{I_+} + \frac{I_+}{I} - 2\right) + c_3 \nu A_+ \left(1 - \frac{I_+}{I}\right) \left(\frac{A}{A_+} - 1\right) \\ & + c_1 \frac{\beta(1-p)}{N_+} \left(1 - \frac{S_+}{S}\right) (I_+ S_+ - IS) + c_2 \frac{\beta(1-p)}{N_+} \left(1 - \frac{A_+}{A}\right) (IS - I_+ S_+), \\ \Phi_4 = & \left[-c_2(\nu + \mu) A_+ + c_1 \beta(1-p) \theta \frac{S_+ A_+}{N_+}\right] \left(\frac{A}{A_+} + \frac{A_+}{A} - 2\right).\end{aligned}$$

First, similar computations as in the proof of the global stability of the disease-free equilibrium Σ_0 show that $\Phi_1 \leq 0$, since $c_1 \omega P_+ = c_4 p \phi S_+$. Next, it is seen that $\Phi_2 \leq 0$, by virtue of the elementary inequality

$$u + \frac{1}{u} - 2 \geq 0, \quad \forall u \in \mathbb{R}.$$

Afterwards, remarking that $(\delta + \mu) I_+ = \nu A_+$, algebraic computations show that $\Phi_3 = \Psi_1 + \Psi_2$ with

$$\begin{aligned}\Psi_1 = & c_3 \nu A_+ \left(3 - \frac{S_+}{S} - \frac{A I_+}{A_+ I} - \frac{A_+ I S}{A I_+ S_+}\right), \\ \Psi_2 = & c_3 \nu A_+ \left(\frac{A}{A_+} + \frac{A_+}{A} - 2\right).\end{aligned}$$

We introduce $u = \frac{S_+}{S}$, $v = \frac{A I_+}{A_+ I}$ and $w = \frac{A_+ I S}{A I_+ S_+}$. It is observed that $uvw = 1$. By virtue of the standard inequality

$$(uvw)^{1/3} \leq \frac{u + v + w}{3},$$

we deduce that $\Psi_1 \leq 0$. Finally, using (7) and (14), we show that $\Phi_4 + \Psi_2 = 0$. Gathering the above results shows that $\dot{V} \leq 0$. Therefore, we have proved that the functional V is a Lyapunov function for the flow induced by the SAIRP model (1). The conclusion follows once again from LaSalle's invariance principle [16]. \square

The theoretical results proved in Theorems 3 and 4 are illustrated in Figure 1.

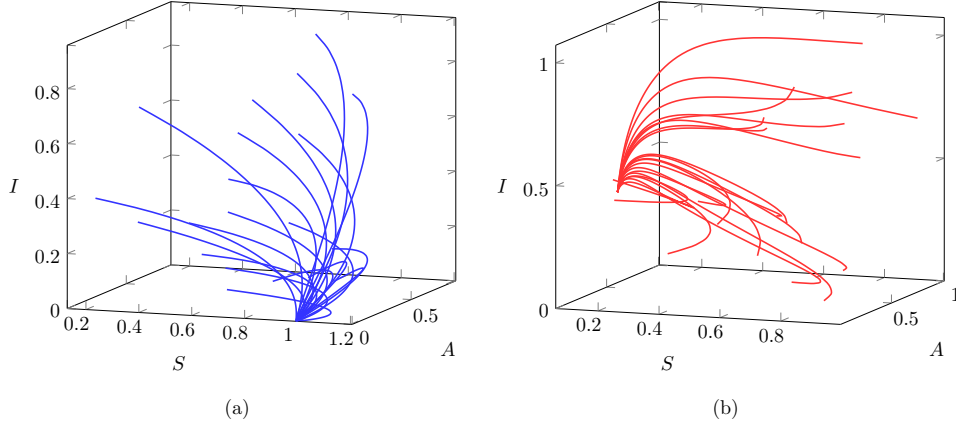


Figure 1: Phase portraits in the (S, A, I) space, illustrating the global stability of the equilibrium points. (a) Global stability of the disease-free equilibrium ($R_0 < 1$). (b) Global stability of the endemic equilibrium ($R_0 > 1$).

3. Model with piecewise constant parameters

The human behavior and the governmental public health decision makers can change the value of the basic reproduction number, R_0 , and consequently the dynamics of model (1). In this section, we model the human behavior and the impact of the decision makers policies, by considering in model (1) parameters determined by piecewise constant functions. We prove the existence and uniqueness of global solutions of the resulting model. We start by subdividing the time line $[0, +\infty)$ into a finite number of n intervals

$$[T_0, T_1) \cup [T_1, T_2) \cup \dots \cup [T_n, +\infty),$$

with disjoint unions, and introduce a piecewise constant function α defined on each time interval as

$$\alpha(t) = \alpha_i, \quad t \in [T_i, T_{i+1}), \quad 0 \leq i \leq n,$$

with $T_0 = 0$, $T_{n+1} = +\infty$ and $\alpha_i \in \mathbb{R}^9$. Next, we consider the sequence of Cauchy problems defined for each initial condition $x_0 \in \Omega$ by

$$\begin{cases} x(0) = x_0, & \dot{x}(t) = f(x(t), \alpha_0), & T_0 < t < T_1, \\ x(T_i) = \lim_{t \rightarrow T_i} x(t), & \dot{x}(t) = f(x(t), \alpha_i), & T_i < t < T_{i+1}, \quad 1 \leq i \leq n. \end{cases} \quad (15)$$

We are now in conditions to derive the existence and uniqueness result.

Proposition 2. *For any initial condition $x_0 \in \Omega$, the sequence of Cauchy problems given by (15) admits a unique global solution, denoted again by $x(t, x_0)$, whose components are non-negative. Furthermore, the region Ω is positively invariant.*

Proof. Applying Theorem 1, a finite number of times, directly provides the existence and uniqueness of global solutions to problem (15). \square

Note that the solutions of problem (15) are continuous on the time interval $[T_0, +\infty)$, but may not be of class \mathcal{C}^1 at $t = T_i$, $0 \leq i \leq n - 1$. From the modeling point of view, each change of parameters occurring at time $t = T_i$ ($1 \leq i \leq n - 1$) corresponds, for example, to a public announcement of confinement/lift of confinement or prohibition of displacement.

4. Existence of pseudo-periodic solutions

In this section, we show that piecewise constant parameters can lead to pseudo-periodic solutions. This result has important practical applications in the context of the COVID-19 pandemic. During the first months of the COVID-19 pandemic, the first concern of governments was to decrease the level of infected individuals. This was achieved, in great part, by confinement decisions. However, those confinement decisions had a large impact on the economy, and it was important to decide to lift this ban. Consequently, the risk of a premature relaxation was the second concern of governments, since it was feared to provoke a second wave of infection. The existence of multiple epidemic waves in a pandemic can be mathematically justified by the following theorem.

Theorem 5. *Assume that the disease-free equilibrium, Σ_0 , admits a non-trivial basin of attraction $\Omega_0 \subset \Omega$ if $R_0 < 1$, and that the endemic equilibrium Σ^+ admits a non-trivial basin of attraction $\Omega^+ \subset \Omega$ if $R_0 > 1$. Let α_0 and α^+ denote two sets of parameters of system (1) such that $R_0(\alpha_0) < 1$ and $R_0(\alpha^+) > 1$. Let $x_0 \in \Omega_0$ and consider the sequence of Cauchy problems*

$$\left\{ \begin{array}{l} x(T_0) = x_0, \quad \dot{x}(t) = f(x(t), \alpha_0), \quad T_0 < t < T_1, \\ x(T_i) = \lim_{\substack{t \rightarrow T_i \\ t \in (T_{i-1}, T_i)}} x(t), \quad \dot{x}(t) = f(x(t), \alpha^+), \quad T_i < t < T_{i+1}, \quad \text{for } i \text{ odd,} \\ x(T_i) = \lim_{\substack{t \rightarrow T_i \\ t \in (T_{i-1}, T_i)}} x(t), \quad \dot{x}(t) = f(x(t), \alpha_0), \quad T_i < t < T_{i+1}, \quad \text{for } i \text{ even,} \end{array} \right. \quad (16)$$

for $1 \leq i \leq n$, where T_i is such that $x(T_i) \in \Omega^+$, for i odd, and $x(T_i) \in \Omega_0$, for i even. Then the solution $x(t, x_0)$, of the latter sequence of Cauchy problems, exhibits pseudo-oscillations between a neighborhood \mathcal{N}_0 of Σ_0 and a neighborhood \mathcal{N}^+ of Σ^+ in Ω .

Proof. The initial condition x_0 of the sequence of Cauchy problems (16) has been chosen in Ω_0 , which is assumed to be the basin of attraction of Σ_0 . Since $\alpha_0(R_0) < 1$, then the solution $x(t, x_0)$ is attracted to Σ_0 and thus reaches a neighborhood \mathcal{N}_0 of Σ_0 after a finite time T_1 . Now it is assumed that $x(T_1)$ belongs to the basin of attraction Ω^+ of Σ^+ . Since $\alpha^+(R_0) > 1$, then the solution $x(t, x_0)$ is now attracted to Σ^+ and thus reaches a neighborhood \mathcal{N}^+ of Σ^+ after a finite time T_2 . Next, we assume that $x(T_2)$ belongs to the basin of attraction Ω_0 of Σ_0 . Since $\alpha_0(R_0) < 1$, then the solution $x(t, x_0)$ is now attracted to Σ_0 and thus reaches again the neighborhood \mathcal{N}_0 of Σ_0 after a finite time T_3 . Repeating those arguments a finite number of times leads to the desired conclusion, that is, the solution $x(t, x_0)$ exhibits pseudo-oscillations between the neighborhoods \mathcal{N}_0 and \mathcal{N}^+ of Σ_0 and Σ^+ , respectively. \square

Note that the assumption $x(T_1) \in \Omega^+$ is directly satisfied for T_1 large enough, if Σ_0 belongs to the interior of Ω^+ in Ω . Similarly, the assumption $x(T_2) \in \Omega_0$ is directly satisfied for T_2 large enough, if Σ^+ belongs to the interior of Ω_0 in Ω . By virtue of Theorem 3, the latter property is directly satisfied since $\Omega_0 = \Omega$. A numerical simulation of a solution of the sequence of Cauchy problems (16), exhibiting pseudo-oscillations between a neighborhood \mathcal{N}_0 of Σ_0 and a neighborhood \mathcal{N}^+ of Σ^+ in Ω , is depicted in Figure 2.

5. Dynamics of a complex network of non-identical SAIRP models

It is now widely admitted that mobilities play an important role on the dynamics of epidemics, at numerous stages of their development. In this section, we propose to study the propagation of the COVID-19 outbreak in Portugal by modeling this country by a complex network in which the six regions studied previously for the calibration of the model (1) are considered.

In a first stage, we show how to construct a complex network of SAIRP models. Let us consider the six regions of Portugal, as depicted in Figure 3. Those six regions are connected by a finite number of links that define a graph $\mathcal{G} = (\mathcal{V}, \mathcal{E})$ made of a set \mathcal{V} of 6 vertices, which correspond to the six regions (*Norte, Centro, Lisboa e Vale do Tejo, Alentejo, Algarve, Pinhal Litoral*), and of a set \mathcal{E} of edges, which model the main connections between those 6 regions. In order to describe

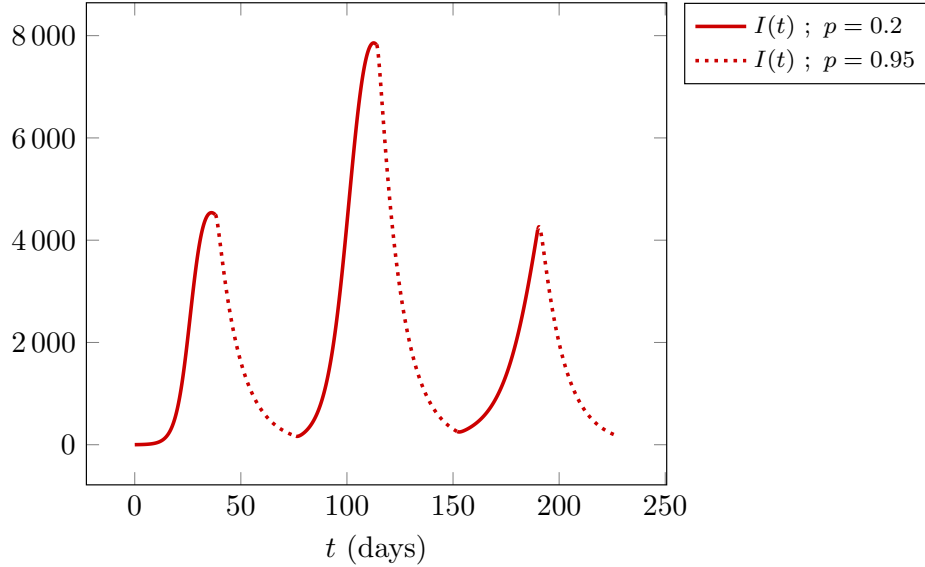


Figure 2: Solution of the sequence of Cauchy problems (16) exhibiting pseudo-oscillations between a neighborhood \mathcal{N}_0 of Σ_0 and a neighborhood \mathcal{N}^+ of Σ^+ in Ω . Here I denotes the number of active infected individuals and p the fraction, $0 < p < 1$, of susceptible individuals S that is transferred to the protected class P .

the state of each region, we couple each vertex of the graph with one instance of the model (15). Since each region has its own specificity, we consider that the multiple instances of the model are non-identical, which means that the values of the parameters can differ from one region to another.

We introduce the following notations:

$$\begin{aligned} x_i &= (S_i A_i, I_i, R_i, P_i)^T \in \mathbb{R}^5, \quad 1 \leq i \leq 6, \\ X &= (x_1, \dots, x_5)^T \in (\mathbb{R}^5)^6, \\ HX &= (Hx_1, \dots, Hx_6)^T \in (\mathbb{R}^5)^6, \\ \alpha(t) &= (\alpha_1(t), \dots, \alpha_6(t)) \in (\mathbb{R}^9)^6, \end{aligned}$$

where H is the matrix of coupling strengths defined by

$$H = \begin{bmatrix} \sigma_S & 0 & 0 & 0 & 0 \\ 0 & \sigma_A & 0 & 0 & 0 \\ 0 & 0 & \sigma_I & 0 & 0 \\ 0 & 0 & 0 & \sigma_R & 0 \\ 0 & 0 & 0 & 0 & \sigma_P \end{bmatrix},$$

with non negative coefficients $\sigma_S, \sigma_A, \sigma_I, \sigma_R$ and σ_P .

Next we define a matrix L of connectivity as follows. For each edge $(k, j) \in \mathcal{E}$, $k \neq j$, we set $L_{j,k} = \varepsilon_{j,k} > 0$. If $(k, j) \notin \mathcal{E}$, $k \neq j$, we set $L_{j,k} = 0$. The diagonal coefficients satisfy

$$L_{j,j} = - \sum_{\substack{k=1 \\ k \neq j}}^n \varepsilon_{k,j},$$

thus L is a matrix whose sums of coefficients in each column is null. For instance, the connectivity

matrix of the graph corresponding to Figure 3 is given by

$$L = \begin{bmatrix} L_{11} & \varepsilon_{12} & 0 & 0 & 0 & \varepsilon_{16} \\ \varepsilon_{21} & L_{22} & \varepsilon_{23} & \varepsilon_{24} & 0 & \varepsilon_{26} \\ 0 & \varepsilon_{32} & L_{33} & \varepsilon_{34} & 0 & \varepsilon_{36} \\ 0 & \varepsilon_{42} & \varepsilon_{43} & L_{44} & \varepsilon_{45} & 0 \\ 0 & 0 & 0 & \varepsilon_{54} & L_{55} & 0 \\ \varepsilon_{61} & \varepsilon_{62} & \varepsilon_{63} & 0 & 0 & L_{66} \end{bmatrix},$$

with

$$\begin{aligned} L_{11} &= -(\varepsilon_{21} + \varepsilon_{61}), \\ L_{22} &= -(\varepsilon_{12} + \varepsilon_{32} + \varepsilon_{42} + \varepsilon_{62}), \\ L_{33} &= -(\varepsilon_{23} + \varepsilon_{43} + \varepsilon_{63}), \\ L_{44} &= -(\varepsilon_{24} + \varepsilon_{34} + \varepsilon_{54}), \\ L_{55} &= -\varepsilon_{45}, \\ L_{66} &= -(\varepsilon_{16} + \varepsilon_{26} + \varepsilon_{36}). \end{aligned}$$

In this complex network model, we consider that an edge $(k, j) \in \mathcal{E}$, $k \neq j$, models a connection between two regions k and j , which corresponds to human displacements from region k towards region j . Moreover, the parameter σ_S models the rate of susceptible individuals in region k which migrate towards vertex j . The parameters σ_A , σ_I , σ_R and σ_P are defined analogously. This implies that our model can take into account the situation where a part of the population is not concerned with the migrations. For instance, it is relevant to consider $\sigma_I = \sigma_P = 0$, while $\sigma_S > 0$ and $\sigma_A > 0$. The set of edges \mathcal{E} and the coupling strengths stored in the matrix H define what is usually called the *topology* of the complex network.

Next, we explicit the equations that describe the state of region $j \in \{1, \dots, 6\}$:

$$\begin{cases} \dot{S}_j = \Lambda_j - \beta_j(1 - p_j) \frac{(\theta_j A_j + I_j)}{N_j} S_j - \phi_j p_j S_j + \omega_j P_j - \mu_j S_j + \sigma_S \sum_{k=1}^5 L_{j,k} S_k, \\ \dot{A}_j = \beta_j(1 - p_j) \frac{(\theta_j A_j + I_j)}{N_j} S_j - \nu_j A_j - \mu_j A_j + \sigma_A \sum_{k=1}^5 L_{j,k} A_k, \\ \dot{I}_j = \nu_j A_j - \delta_j I_j - \mu_j I_j + \sigma_I \sum_{k=1}^5 L_{j,k} I_k, \\ \dot{R}_j = \delta_j I_j - \mu_j R_j + \sigma_R \sum_{k=1}^5 L_{j,k} R_k, \\ \dot{P}_j = \phi_j p_j S_j - \omega_j P_j - \mu_j P_j + \sigma_P \sum_{k=1}^5 L_{j,k} P_k, \end{cases} \quad (17)$$

where the time dependence is omitted, in order to lighten the notations. In particular, the parameters can be determined by piecewise constant functions as in model (15).

In the next theorem, we establish the existence and uniqueness of global solutions to the complex network problem (17) as for models (1) and (15). Following [7], we introduce the minimum mortality rate μ_0 defined by

$$\mu_0 = \min_{1 \leq j \leq 6} \mu_j,$$

the positive coefficient Λ_0 defined by

$$\Lambda_0 = \sum_{j=1}^6 \Lambda_j,$$

and the compact region

$$\Theta = \left\{ (x_j)_{1 \leq j \leq 30} \in (\mathbb{R}^+)^{30} ; \sum_{j=1}^{30} x_j \leq \frac{\Lambda_0}{\mu_0} \right\}. \quad (18)$$

Theorem 6. *For any $X_0 \in \Theta$, the Cauchy problem given by (17) and $X(0) = X_0$ admits a unique solution denoted by $X(t, X_0)$, defined on $[0, \infty)$, whose components are non-negative. Furthermore, the region Θ defined by (18) is positively invariant.*

Proof. The existence and uniqueness of local in time solutions is immediate. The non-negativity property is guaranteed by the quasi-positivity of the non-linear operator determined by the right hand side of system (17). The total population in the complex network, defined by

$$N(t) = \sum_{j=1}^6 [S_j(t) + A_j(t) + I_j(t) + R_j(t) + P_j(t)], \quad t \geq 0,$$

satisfies

$$\dot{N}(t) \leq -\mu_0 N(t) + \Lambda_0, \quad t \geq 0,$$

since the matrix of connectivity L is a zero column sum matrix. It follows that

$$N(t) \leq \left[N(0) - \frac{\Lambda_0}{\mu_0} \right] e^{-\mu_0 t} + \frac{\Lambda_0}{\mu_0}, \quad t \in [0, T],$$

which leads to the intended conclusion. \square

In the next section, we apply previous complex network to the real data from COVID-19 in Portugal, since the first confirmed active COVID-19 case, in March 2, 2020, until September 17, 2020.

6. Portugal case study: complex network with 6 regions

In this section, we calibrate the number of active infected individuals I given by the *SAIRP* model with piecewise constant parameters (15), to six distinct regions from Portugal. We show that the model allows to fit well the Portuguese real data available in [2]. Taking into account these parameter values, we perform numerical simulations of the complex network problem (17), where the main goal is to investigate the effect of the topology on the dynamics of the epidemics, and determine a topology that minimizes the level of active infected individuals.

6.1. Model with piecewise constant parameters: fitting to real data from 6 Portuguese regions

We first consider the *SAIRP* model with piecewise constant parameters (15) and show that the class I fits well the active confirmed cases of infected individuals provided by the Portuguese National Authorities [2] for six regions of Portugal mainland, as depicted in Figure 3, where (1) represents the region *Norte*, (2) *Centro*, (3) *Lisboa e Vale do Tejo*, (4) *Alentejo*, (5) *Algarve* and (6) *Pinhal Litoral*.

The initial conditions S_0 , A_0 , I_0 , R_0 and P_0 at time $t = 1$, where $t = 1$ corresponds to the day of the first confirmed cases of COVID-19 disease in each region, which differ from one region to another, see Table 1. Namely, the first cases occurred in each region at: *Norte*, March 2, 2020; *Centro*, March 3, 2020; *Lisboa e Vale do Tejo*, March 3, 2020; *Alentejo*, March 18, 2020; *Algarve*, March 8, 2020.

Some of the parameters take constant values for all the period of time under consideration and are the same for the six regions, see Table 2. Others, even taking constant values for all time window, differ from one region to another, see Table 3.

The parameters β , m and p are piecewise continuous, taking different values depending on the considered time interval and the region, see Tables 4 and 5.

Figures 4–6 show that the *SAIRP* model (15) with piecewise constant parameters describes well the active infected cases in the six Portuguese regions under consideration.

Moreover, the active infected cases of all Portugal can also be modeled, see Figure 7.

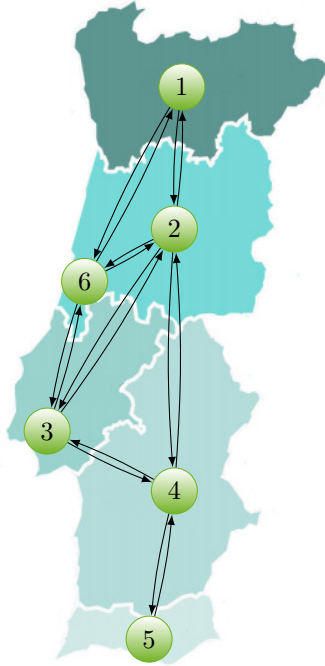


Figure 3: Six regions of Portugal and some of their connections: (1) *Norte*; (2) *Centro*; (3) *Lisboa e Vale do Tejo*; (4) *Alentejo*; (5) *Algarve*; (6) *Pinhal litoral*.

Table 1: Initial conditions for each of the six regions in Portugal.

Region	S_0	A_0	I_0	R_0	P_0
<i>Norte</i>	3125804	2	$\frac{2}{0.15}$	0	0
<i>Centro</i>	1480664	1	$\frac{1}{0.15}$	0	0
<i>Lisboa e Vale do Tejo</i>	3659871	1	$\frac{1}{0.15}$	0	0
<i>Alentejo</i>	166726	2	$\frac{2}{0.15}$	0	0
<i>Algarve</i>	451006	1	$\frac{1}{0.15}$	0	0
<i>Pinhal litoral</i>	271078	3	$\frac{3}{0.15}$	0	0

Table 2: Constant parameter values that take the same values for the six regions, in Portugal.

Parameter	Description	Value	Reference
Λ	Recruitment rate	$\frac{0.19\% \times N_0}{365}$	[21]
μ	Natural death rate	$\frac{1}{81 \times 365}$	[21]
θ	Modification parameter	1	[23]
v	Transfer rate from A to I	1	[23]
q	Fraction of A individuals that are confirmed to be infected	0.15	[23]

6.2. Complex network model: numerical simulations for COVID-19 in Portugal

Considering the six regions from Figure 3, and the parameter values from Section 6.1, we perform numerical simulations of the complex network problem (17). The main goal is to investigate the effect of the topology on the dynamics of the epidemics. In particular, we analyze the existence of a topology which minimizes the average number of active infected individuals during a fixed time interval. Moreover, we analyze if other topologies are likely to worsen the level of infection.

In order to model the mobilities of susceptible and asymptomatic individuals, we set $\sigma_S = \sigma_A > 0$, whereas we fix $\sigma_I = \sigma_R = \sigma_P = 0$. We test a sample of 1000 randomly generated topologies

Table 3: Constant parameter values that differ from one region to another, in Portugal.

Region	ϕ (transfer rate from S to P)	δ (transfer rate from I to R)	w (transfer rate from P to S)
<i>Norte</i>	$\phi = \frac{1}{12}$	$\delta = \frac{1}{27}$	$w = \frac{1}{45}$
<i>Centro</i>	$\phi = \frac{1}{11}$	$\delta = \frac{1}{27}$	$w = \frac{1}{45}$
<i>Lisboa e Vale do Tejo</i>	$\phi = \frac{1}{11}$	$\delta = \frac{1}{27}$	$w = \frac{1}{45}$
<i>Alentejo</i>	$\phi = 1$	$\delta = \frac{1}{21}$	$w = \frac{1}{41}$
<i>Algarve</i>	$\phi = \frac{1}{6}$	$\delta = \frac{1}{21}$	$w = \frac{1}{45}$
<i>Pinhal litoral</i>	$\phi = 1$	$\delta = \frac{1}{21}$	$w = \frac{1}{43}$

Table 4: Piecewise constant parameter values for the regions *Norte*, *Centro* and *Lisboa e Vale do Tejo*

Region	β (transmission rate)	p (transfer fraction from S to P)	m (transfer fraction from P to S)
Norte			
Time interval: [1; 75]	$\beta_1 = 1.40$	$m_1 = 0.09$	$p_1 = 0.675$
Time interval: [75; 122]	$\beta_2 = 0.15$	$m_2 = 0.15$	$p_2 = 0.60$
Time interval: [122; 170]	$\beta_3 = 1.28$	$m_3 = 0.14$	$p_3 = 0.56$
Time interval: [170; 200]	$\beta_4 = 1.46$	$m_4 = 0.17$	$p_4 = 0.52$
Centro			
Time interval: [1; 69]	$\beta_1 = 1.351$	$m_1 = 0.10$	$p_1 = 0.675$
Time interval: [69; 94]	$\beta_2 = 0.45$	$m_2 = 0.09$	$p_2 = 0.60$
Time interval: [94; 164]	$\beta_3 = 1.10$	$m_3 = 0.16$	$p_3 = 0.56$
Time interval: [164; 199]	$\beta_4 = 1.33$	$m_4 = 0.17$	$p_4 = 0.54$
Lisboa e Vale do Tejo			
Time interval: [1; 36]	$\beta_1 = 1.45$	$m_1 = 0.16$	$p_1 = 0.675$
Time interval: [36; 54]	$\beta_2 = 1.13$	$m_2 = 0.13$	$p_2 = 0.69$
Time interval: [54; 129]	$\beta_3 = 1.41$	$m_3 = 0.13$	$p_3 = 0.56$
Time interval: [129; 160]	$\beta_4 = 1.10$	$m_4 = 0.11$	$p_4 = 0.57$
Time interval: [160; 199]	$\beta_5 = 1.43$	$m_5 = 0.17$	$p_5 = 0.54$

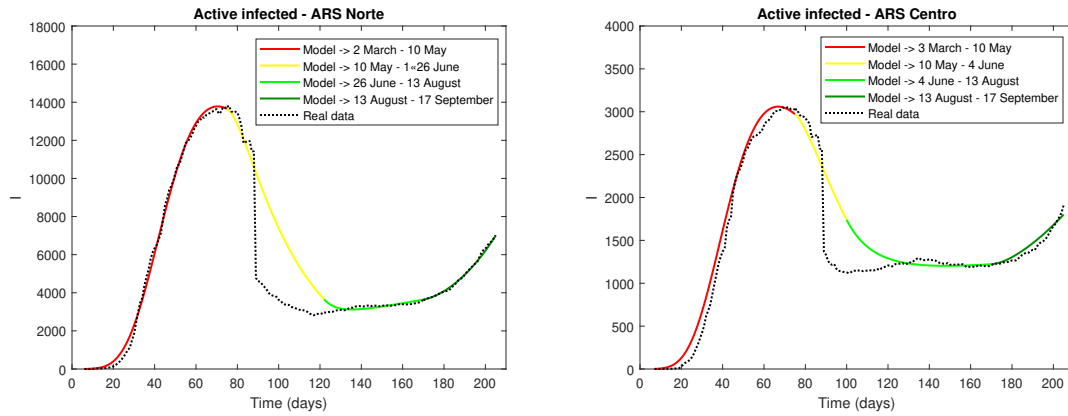


Figure 4: Active infected cases of COVID-19. The black dotted lines represent the real data and the continuous lines represent the active infected individuals, I , output of the *SAIRP* model with piecewise constant parameters from Table 4. Left: region *Norte*. Right: region *Centro*.

among 2^{16} topologies (*id est* sets of edges), for $\sigma_S = \sigma_A \in [0.01, 0.1]$. For each randomly generated topology, we perform a numerical integration of the complex network problem (17), with the same

Table 5: Piecewise constant parameter values for the regions *Alentejo*, *Algarve* and *Pinhal Litoral*

Region	β (transmission rate)	p (transfer fraction from S to P)	m (transfer fraction from P to S)
Alentejo			
Time interval: [1; 11]	$\beta_1 = 3.50$	$m_1 = 0.40$	$p_1 = 0.675$
Time interval: [11; 29]	$\beta_2 = 7.80$	$m_2 = 0.45$	$p_2 = 0.45$
Time interval: [29; 84]	$\beta_3 = 4.40$	$m_3 = 0.38$	$p_3 = 0.55$
Time interval: [84; 104]	$\beta_4 = 6.90$	$m_4 = 0.46$	$p_4 = 0.48$
Time interval: [104; 124]	$\beta_5 = 2.70$	$m_5 = 0.30$	$p_5 = 0.56$
Time interval: [124; 184]	$\beta_6 = 4.10$	$m_6 = 0.36$	$p_6 = 0.44$
Algarve			
Time interval: [1; 36]	$\beta_1 = 1.11$	$m_1 = 0.10$	$p_1 = 0.60$
Time interval: [36; 69]	$\beta_2 = 1.37$	$m_2 = 0.20$	$p_2 = 0.52$
Time interval: [69; 91]	$\beta_3 = 0.80$	$m_3 = 0.20$	$p_3 = 0.55$
Time interval: [91; 109]	$\beta_4 = 1.90$	$m_4 = 0.32$	$p_4 = 0.45$
Time interval: [109; 149]	$\beta_5 = 1.35$	$m_5 = 0.22$	$p_5 = 0.58$
Time interval: [149; 194]	$\beta_6 = 1.35$	$m_6 = 0.30$	$p_6 = 0.55$
Pinhal litoral			
Time interval: [1; 7]	$\beta_1 = 3.00$	$m_1 = 0.09$	$p_1 = 0.675$
Time interval: [7; 23]	$\beta_2 = 8.15$	$m_2 = 0.25$	$p_2 = 0.44$
Time interval: [23; 77]	$\beta_3 = 5.00$	$m_3 = 0.16$	$p_3 = 0.55$
Time interval: [77; 115]	$\beta_4 = 7.80$	$m_4 = 0.25$	$p_4 = 0.42$
Time interval: [115; 145]	$\beta_5 = 4.15$	$m_5 = 0.15$	$p_5 = 0.52$
Time interval: [145; 186]	$\beta_6 = 7.75$	$m_6 = 0.27$	$p_6 = 0.42$

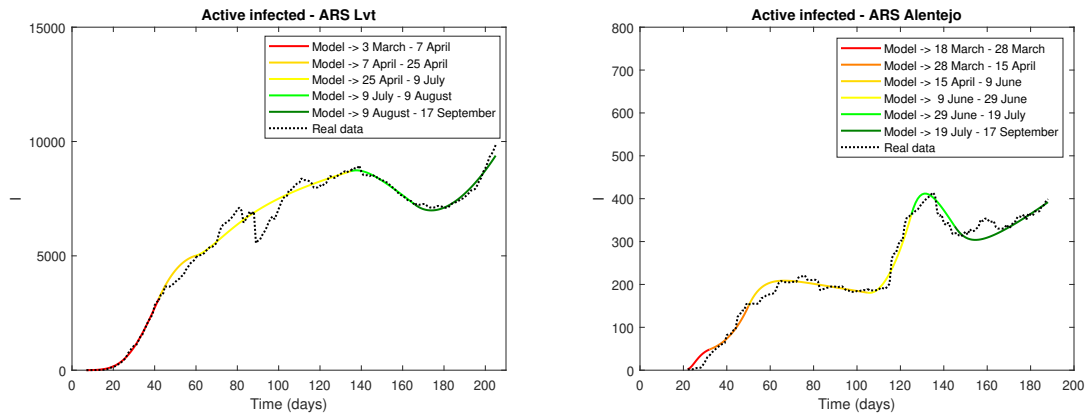


Figure 5: Active infected cases of COVID-19. The black dotted lines represent the real data and the continuous lines represent the active infected individuals, I , output of the *SAIRP* model with piecewise constant parameters from Tables 4–5. Left: region *Lisboa e Vale do Tejo*. Right: region *Alentejo*.

parameters $\alpha_1, \alpha_2, \dots, \alpha_6$ as considered in Section 6.1. The computation has been performed with `Python 3.5` language, in a Debian/Gnu-Linux environment. For each integration, we have computed the number of average number of active infected individuals, that is, individuals of the class I , per day. The results are depicted in Figure 8, where the average number of active infected individuals, per day, is depicted for the randomly generated topologies and $\sigma_S = \sigma_A = 0.01$, and in Figure 9, where the average number of active infected individuals is depicted with respect to the coupling strengths $\sigma_S = \sigma_A$ for a couple of remarkable topologies. The numerical results reveal the existence of a certain number of topologies that decrease the level of infection, compared to

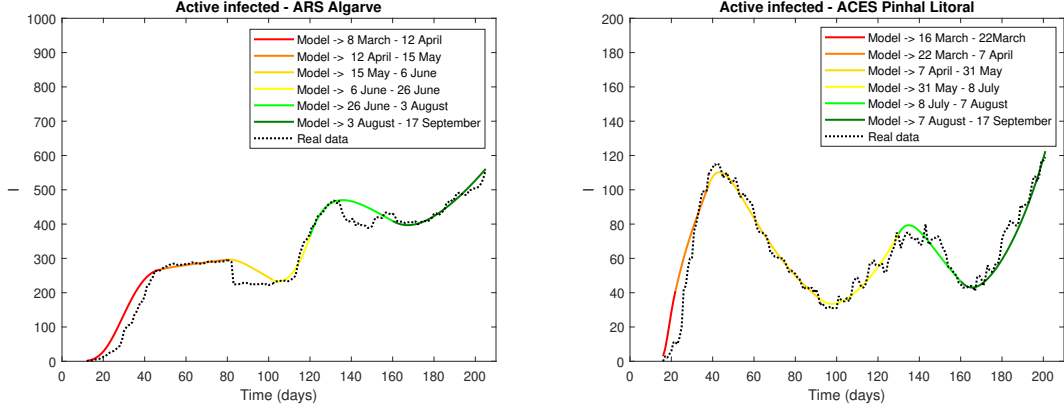


Figure 6: Active infected cases of COVID-19. The black dotted lines represent the real data and the continuous lines represent the active infected individuals, I , output of the *SAIRP* model with piecewise constant parameters from Table 5. Left: region *Algarve*. Right: region *Pinhal litoral*.

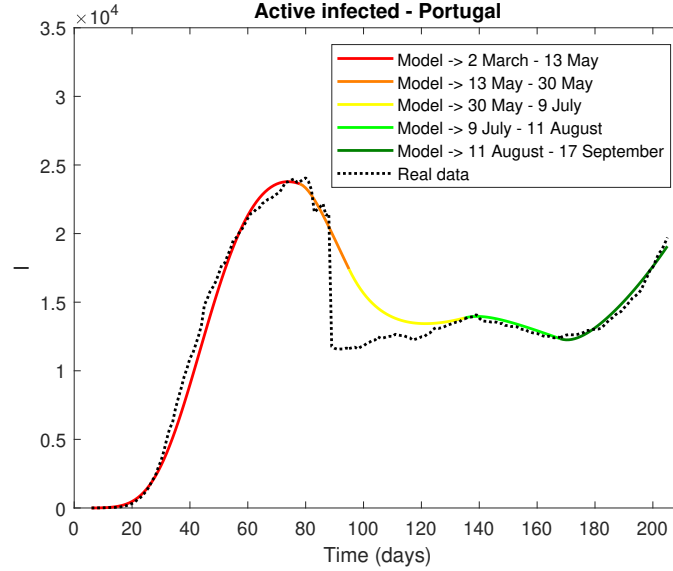


Figure 7: Active infected cases of COVID-19 in Portugal. The black dotted lines represent the real data and the continuous lines represent the active infected individuals, I , output of the *SAIRP* model with piecewise constant parameters. Initial conditions: $S_0 = 10295894$, $I_0 = 2$, $A_0 = \frac{2}{0.15}$, $R_0 = 0$, $Q_0 = 0$. The constant parameters take the values $\phi = 1$, $\delta = \frac{1}{27}$, $w = \frac{1}{45}$ and the remaining constant parameters take the values in Table 2. The first infected case with COVID-19 in Portugal, $t = 1$, occurred on March 2, 2020. Piecewise constant parameters: $t \in [1; 73]$, $\beta_1 = 1.505; m_1 = 0.09; p_1 = 0.675$; $t \in [73; 90]$, $\beta_2 = 0.50; m_2 = 0.09; p_2 = 0.65$; $t \in [90; 130]$, $\beta_3 = 1.15; m_3 = 0.18; p_3 = 0.58$; $t \in [130; 163]$, $\beta_4 = 0.96; m_4 = 0.16; p_4 = 0.61$; $t \in [163; 200]$, $\beta_5 = 1.50; m_5 = 0.17; p_5 = 0.58$.

the empty topology, which corresponds to the situation where individuals do not migrate from one region to another. Among those topologies, one minimizes the level of cumulated infected individuals. This optimal topology is depicted in Figure 10 (b). It is worth noting that this optimal topology connects the regions *Norte*, *Centro*, *Lisboa e Vale do Tejo* and *Pinhal Litoral*, but it does not connect those four regions to *Alentejo* and *Algarve*. In parallel, the numerical simulations exhibit numerous topologies that increase the level of infection. We have presented in

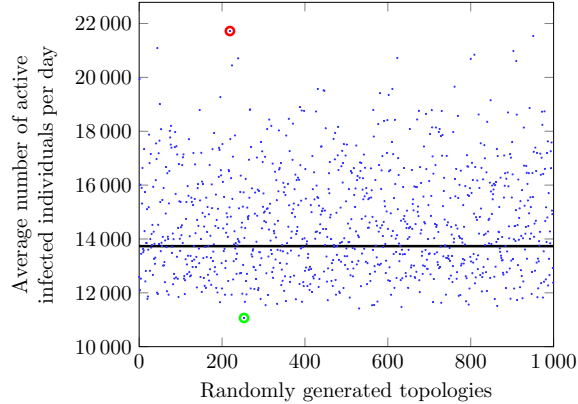


Figure 8: Average number of active infected individuals, per day, for a sample of 1000 randomly generated topologies, for $\sigma_S = \sigma_A = 0.01$. The black line shows the level of infection for the empty topology. The green circle shows the optimum topology which minimizes the level of infection, whereas the red circle shows the topology which leads to the highest level of infection.

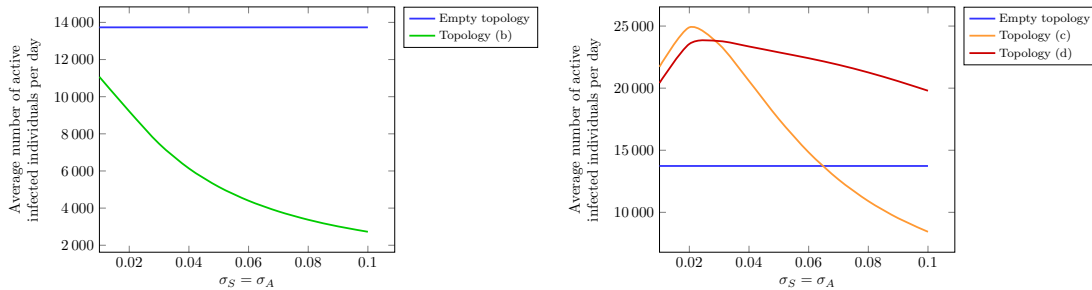


Figure 9: Average number of active infected individuals, for each topology, with respect to the coupling strengths $\sigma_S = \sigma_A$. Left: optimum topology which minimizes the level of infection of the epidemics. Right: two examples of topologies that can increase the level of infection, compared to the empty topology, which corresponds to the situation where individuals do not migrate from one region to another. Topology (c) leads to a level of infection that overcomes the level of the empty topology for only a weak coupling strength, whereas topology (d) seems to permanently overcome the level of the empty topology.

Figure 10 (c) and (d) two examples of such topologies. The corresponding levels of infection are presented in Figure 9. Topology (c) leads to a level of infection that overcomes the level of the empty topology for only a weak coupling strength, whereas topology (d) seems to permanently overcome the level of the empty topology. We remark that the topologies that increase the level of infection seem to connect the 6 regions of Portugal to the region *Alentejo*. On the other hand, it can be helpful to authorize parsimonious migrations between regions that have a satisfying control of the epidemic.

7. Discussion

One of the factors associated with the spread of the pandemic is the mobility of populations. It was based on this evidence that, in the first phase of the pandemic response, a generalized containment of the population was implemented in a big number of countries. As a result of this restriction in the mobility, it was possible to obtain a decrease in the number of infected. In the numerical simulations considered in this work, for the complex network problem (17), it is

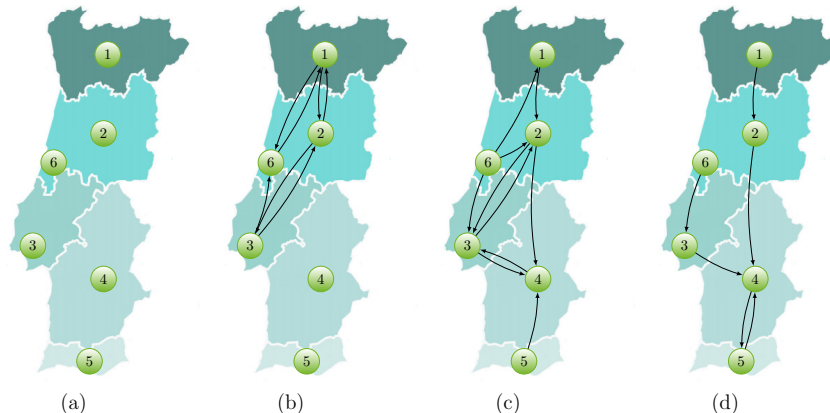


Figure 10: Four remarkable topologies. (a) Empty topology, which corresponds to the situation where individuals do not migrate from one region to another. (b) Topology that minimizes the level of infection. (c) Topology that leads to a level of infection greater than the level of the empty topology for only a weak coupling strength. (d) Topology that permanently overcomes the level of the empty topology.

assumed that only susceptible (S) and asymptomatic infected (A) are circulating among the 6 identified regions of mainland Portugal. Starting from the number of active infected people (I) for the empty topology, in which it is assumed that there are no flows between regions, the results of the simulations indicate that there are more topologies that increase the number of active infected people than those that cause this number to decrease. Hence, this result reinforces the need to reduce circulation between regions as one of the tools to reduce the spread of the virus and decrease the number of active infected people. Still, it is interesting to note that there are other topologies (around 1 out of 3) in which the number of active infected individuals decreases with the movement of people between regions. This finding can be seen in Figure 8, where the average number of active infected individuals for the 1000 tested topologies is shown. According to the topology that minimizes the number of active infected individuals, whose representation is shown in Figure 10 b), it is possible to verify that the strategy of preventing the flow to the regions of *Alentejo* (4) and *Algarve* (5) contributes to reduce the number of active infected. This scenario was to be expected as those regions have a much lower number of cases than the rest of Portugal. Bidirectional circulation between *Norte* (1) and *Centro* (2) regions leads to a reduction in the number of active infected people (if one compares with the empty topology), but the movement between *Pinhal Litoral* region (6) and *Lisboa e Vale do Tejo* region (3) should only be done in the direction to prevent circulation from the region where there are less infected (6) to the region (3) that has a high number of active cases. In Figure 10 c) it is possible to verify that the existence of this connection in the direction (6) to (3) increases the number of active cases. The topologies involving the regions of *Alentejo* (4) and *Algarve* (5) increase the number of cases. One extreme example of such topology can be found in Figure 10 d). In this case, the direction of the flows presents a topology that converges to the *Alentejo* (4) and it is expected that this will translate into an increase in the number of infected (even in the case where the connection strength is small, as shown in Figure 10 c) and Figure 9 at right), as it is the region where the number of cases is lesser. The way the epidemic evolves is different between the different regions of a country, but also between countries. These specific characteristics of context (cultural, demographic, economic, ...) seen in the number of active infected individuals (which is not uniform across regions), can be modeled by pseudo-periodic piecewise functions, as proved in this work. Accordingly, the application of such methodology to identify flows between regions or countries is a tool with enormous potential in the current pandemic context, and can be applied in the management of outbreaks (in regional terms) but also to manage the opening/closing of borders.

8. Conclusion and future work

The way the epidemic evolves is different between the different regions of a country, but also between countries. These specific characteristics of context (cultural, demographic, economic, . . .) seen in the number of active infected individuals, which is not uniform across regions, can be modeled by pseudo-periodic piecewise functions, as proved in this work. Accordingly, the application of such methodology to identify flows between regions or countries is a tool with enormous potential in the current pandemic context, and can be applied in the management of outbreaks (in regional terms) but also to manage the opening/closing of borders. In the implemented simulations, the intensity of the flows (σ_S and σ_A) are assumed to be equal. Still, and as future work, it would be useful, in terms of epidemiological management, to be able to model the intensity of flows by class (Asymptomatic, Susceptible, Active Infected, Recovered, and Protected) between regions.

Acknowledgments

This research is partially supported by the Portuguese Foundation for Science and Technology (FCT) within “Project Nr. 147 – Controlo Ótimo e Modelação Matemática da Pandemia COVID-19: contributos para uma estratégia sistémica de intervenção em saúde na comunidade”, in the scope of the “RESEARCH 4 COVID-19” call financed by FCT, and by project UIDB/04106/2020 (CIDMA). Silva is also supported by national funds (OE), through FCT, I.P., in the scope of the framework contract foreseen in the numbers 4, 5 and 6 of the article 23, of the Decree-Law 57/2016, of August 29, changed by Law 57/2017, of July 19. Rui Fonseca-Pinto and Rui Passadouro are supported by the FCT projects UIDB/05704/2020 and UIDP/05704/2020.

References

- [1] Benjamin Ambrosio and M. A. Aziz-Alaoui. On a coupled time-dependent SIR models fitting with New York and New-Jersey states Covid-19 data. *arXiv preprint*, 2020. [arXiv:2006.05665](https://arxiv.org/abs/2006.05665)
- [2] Direção Geral da Saúde COVID-19. Ponto de situação atual em Portugal, 2020.
- [3] M. A. Aziz-Alaoui. Synchronization of chaos. *Encyclopedia of Mathematical Physics*, 5:213–226, 2006.
- [4] Arnaud Banos, Nathalie Corson, Benoit Gaudou, Vincent Laperrière, and Sébastien Rey Coyrehourcq. The importance of being hybrid for spatial epidemic models: a multi-scale approach. *Systems*, 3(4):309–329, 2015.
- [5] Vladimir N. Belykh, Igor V. Belykh, and Martin Hasler. Connection graph stability method for synchronized coupled chaotic systems. *Physica D: nonlinear phenomena*, 195(1-2):159–187, 2004.
- [6] G. Cantin. Non identical coupled networks with a geographical model for human behaviors during catastrophic events. *International Journal of Bifurcation and Chaos*, 27(14):1750213, 2017.
- [7] G. Cantin and Cristiana J. Silva. Influence of the topology on the dynamics of a complex network of HIV/AIDS epidemic models. *AIMS Mathematics*, 4:1145, 2019.
- [8] Dawit Denu, Sedar Ngoma, and Rachidi B. Salako. Existence of traveling wave solutions of a deterministic vector-host epidemic model with direct transmission. *Journal of Mathematical Analysis and Applications*, 487(1):123995, 2020.
- [9] Joshua M. Epstein, Jon Parker, Derek Cummings, and Ross A. Hammond. Coupled contagion dynamics of fear and disease: mathematical and computational explorations. *PLoS One*, 3(12):e3955, 2008.

- [10] Euronews. Coronavirus second wave: Which countries in Europe are experiencing a fresh spike in COVID-19 cases?, 2020.
- [11] Centers for Disease Control and Prevention. Coronavirus disease 2019 (COVID-19), 2020.
- [12] European Centre for Disease Prevention and Control. Guidelines for the implementation of non-pharmaceutical interventions against COVID-19, 2020.
- [13] Martin Golubitsky and Ian Stewart. Nonlinear dynamics of networks: the groupoid formalism. *Bulletin of the American Mathematical Society*, 43(3):305–364, 2006.
- [14] Cheng-Hsiung Hsu and Jian-Jhong Lin. Stability of traveling wave solutions for nonlinear cellular neural networks with distributed delays. *Journal of Mathematical Analysis and Applications*, 470(1):388–400, 2019.
- [15] Steven G. Krantz and Arni S. R. Srinivasa Rao. Level of underreporting including underdiagnosis before the first peak of COVID-19 in various countries: Preliminary retrospective results based on wavelets and deterministic modeling. *Infection control and hospital epidemiology*, pages 1–3, 2020.
- [16] Joseph LaSalle. Some extensions of liapunov’s second method. *IRE Transactions on circuit theory*, 7(4):520–527, 1960.
- [17] N. Moradian, H. D. Ochs, C. Sedikies et al. The urgent need for integrated science to fight COVID-19 pandemic and beyond. *J. Transl. Med.*, 205, 2020.
- [18] Faiçal Ndairou, Iván Area, Juan J. Nieto, and Delfim F. M. Torres. Mathematical modeling of COVID-19 transmission dynamics with a case study of Wuhan. *Chaos, Solitons & Fractals*, 135:109846, 2020. [arXiv:2004.10885](https://arxiv.org/abs/2004.10885)
- [19] World Health Organization. WHO announces COVID-19 outbreak a pandemic, 2020.
- [20] Lawrence Perko. *Differential equations and dynamical systems*, volume 7. Springer Science & Business Media, 2013.
- [21] Pordata. Taxa de crescimento anual médio segundo os censos (%), 2020.
- [22] Kankan Sarkar, Subhas Khajanchi, and Juan J. Nieto. Modeling and forecasting the COVID-19 pandemic in India. *Chaos, Solitons & Fractals*, 139:110049, 2020.
- [23] Cristiana J. Silva, Carla Cruz, Delfim F. M. Torres, Alberto P. Muñozuri, Alejandro Carballosa, Ivan Area, Juan J. Nieto, Rui Fonseca-Pinto, Rui Passadouro da Fonseca, Estevão Soares dos Santos, Wilson Abreu, and Jorge Mira. Optimal control of the COVID-19 pandemic: controlled sanitary deconfinement in Portugal. *Submitted*, 2020, Preprint: <https://arxiv.org/abs/2009.00660>. [arXiv:2009.00660](https://arxiv.org/abs/2009.00660)
- [24] Hal L. Smith and Horst R. Thieme. *Dynamical systems and population persistence*, volume 118. American Mathematical Soc., 2011.
- [25] Pauline van den Driessche and James Watmough. Reproduction numbers and sub-threshold endemic equilibria for compartmental models of disease transmission. *Mathematical Biosciences*, 180(1-2):29–48, 2002.
- [26] Marco Vinceti, Tommaso Filippini, Kenneth J Rothman, Fabrizio Ferrari, Alessia Goffi, Giuseppe Maffei, and Nicola Orsini. Lockdown timing and efficacy in controlling COVID-19 using mobile phone tracking. *EClinicalMedicine*, 25(100457), 2020.
- [27] Zhi-Cheng Wang and Jianhong Wu. Traveling waves of a diffusive Kermack–McKendrick epidemic model with non-local delayed transmission. *Proceedings of the Royal Society A: Mathematical, Physical and Engineering Sciences*, 466(2113):237–261, 2010.